Viscoelastic Polymer Flow, Past a Cylinder: CFD Investigation and Regression Analysis

Abdulaal Zuhayr Al Khazaal*

Department of Chemical & Materials Engineering, College of Engineering, Northern Border University, Arar, Saudi Arabia

*Corresponding author; E-mail: abdulaal.akhazaal@nbu.edu.sa

Abstract:

Viscoelastic polymer flow past a circular cylinder was investigated via twodimensional steady CFD simulations using the Oldroyd-B constitutive model. The study covered creeping-to-low Reynolds regimes (Re = 0.001-5) and moderate elasticity (Weissenberg number Wi = 0-1). The computed flow fields show that polymer elasticity significantly alters the pressure and stress distribution. In particular, the polymeric normal stress (τ_{xx}) builds up strongly at the cylinder wall and along the downstream wake centerline, yielding two pronounced stress maxima, one in the boundary layer and one in the wake, in agreement with classical viscoelastic flow results. As Wi increases, the drag coefficient Cd decreases from its Newtonian value, reaching a minimum at an intermediate Wi (≈0.6) before a slight rebound at the highest Wi. For example, compared to the Newtonian case (Wi=0), we observe a steady drag reduction on the order of 10–20% at peak elasticity. A nonlinear regression model was fitted to the CFD data to predict Cd as a function of Re and Wi. The resulting surrogate has excellent accuracy (R2=0.99586, with low MSE, RMSE and MAE), capturing the complex Re-Wi dependence of drag. This combined CFD-regression approach thus provides a fast, reliable estimator for cylinder drag.

Key words: Oldroyd-B flow; cylinder drag; polymer stress; viscoelastic CFD; regression model.

1. INTRODUCTION

Chemical engineers, fluid mechanics, and polymer engineers are just a few of the scientific and commercial domains that have shown keen interest in the behavior of viscoelastic polymer flows around a circular cylinder. The complex interaction between the fluid's elastic characteristics and inertial factors causes this flow phenomenon. Many studies have tried to decipher this flow characteristic. Research has demonstrated time and time again that, in comparison to a Newtonian fluid, the drag coefficient is substantially reduced due to the fact that polymers' elasticity considerably influences the distribution of pressure and stress across the cylinder. In their study of Giesekus viscoelastic fluids flowing around a cylinder, Owens and Phillips (2002) found that, compared to the Newtonian case, there was a drag reduction of 30%. In their simulation of Oldroyd-B fluids flowing around a cylinder, Harlen et al. (1990)

showed that there are two separate normal stress peaks, one in the boundary layer and another in the wake. These peaks explain the observed decrease in drag. Similar findings were reported in studies by Chhabra and Richardson (1999), who emphasized the role of elasticity in modifying stress distributions. The researchers have been looking into how viscoelasticity affects the flow dynamics surrounding bluff bodies, which is consistent with the findings of earlier studies into this topic. Binding and Walters (1998) explored the computational and experimental flow of viscoelastic fluids around spherical cylinders, while Chhabra and Richardson (1999) investigated the influence of normal stress fluctuations on pressure distribution. According to the findings of their investigation, the wake structure was very different from that of Newtonian fluids. In the context of cylinder-bound Boger fluid flow, Baaijens et al. (1997) demonstrated that there is a significant link between the drag coefficient and the Deborah number, which is a metric that measures elasticity. A recent numerical investigation by Sun et al. (2014) focused on the effect of increasing Reynolds and Weissenberg numbers on the drag coefficient, pressure distribution, and flow patterns around a cylinder-bound viscoelastic fluid. Their results showed that as the Weissenberg number increased, the drag coefficient experienced a significant decrease, which they attributed to the formation of elongated vortices.

In spite of the significant study that has been conducted in this field, the underlying physical mechanisms that are responsible for the phenomenon of aerodynamic drag reduction are still not fully understood. Through the utilization of a computational fluid dynamics (CFD) methodology that is based on finite elements and nonlinear regression analysis, the purpose of this work is to improve the understanding of viscoelastic flows that occur around a cylinder. These three objectives constitute the primary goals of this endeavor:

- 1. The purpose of this study is to investigate the influence that the Weissenberg number (Wi), which is suggestive of the fluid's elasticity, and the Reynolds number (Re), which is reflective of the inertial effects, have on flow fields, pressure and stress distributions, and the drag coefficient. By conducting this experiment, substantial insights into the physical reasons that are responsible for the decrease in drag that was observed in previous tests will be obtained (Larson et al. (1992), Shaqfeh et al. (1996) and McKinley et al. (1999)).
- 2. With the help of the data obtained from computational fluid dynamics (CFD) simulations, the objective is to develop a nonlinear regression model that is capable of accurately and rapidly predicting the drag coefficient as a function of Wi and Re (Zhang et al. (2014), Rallison et al. (1988)). This model would serve as an effective and dependable predictive tool, which would be advantageous for improving industrial processes that are associated with this flow type and for developing reduced-order models in parametric research (Pearson (1985) and Phan-Thien et al. (1977)).
- 3. The objective is to conduct a thorough evaluation of the statistical validity of the developed regression model by determining how well it fits the CFD data and studying the characteristics of the residuals through a rigorous assessment process (Bird, R. B., et al. (1987) and Poole et al. (2009)). Because of this, the model will be able to accurately reflect the complex nonlinear relationship that exists between the drag coefficient, Wi, and Re.

With the help of computational fluid dynamics (CFD) and regression analysis techniques, the purpose of this research is to improve the understanding of the physical principles that govern viscoelastic flow around a cylinder. Additionally, the study aims to develop a tool that is both reliable and quick in its ability to forecast drag coefficients. According to the findings of this study, it is possible that the optimization of industrial processes that are associated with this kind of flow and the development of reduced-order models in parametric investigations will be advantageous (Keunings, R. (1986), White & Mungal (2008), Tanna & Zaki (2016), Bonn et al. (2004) and Tropea, et al. (2007)).

2. PROBLEM DESCRIPTION AND GOVERNING EQUATIONS

The computational domain (Figure 1) consists of a two-dimensional horizontal channel with a circular cylinder mounted at its centerline. The cylinder is fixed, and the flow of the Oldroyd-B fluid, capturing both the solvent's viscous response and the elastic effects of polymeric additives, is symmetric about the centerline. Due to the symmetry of the problem, only the upper half of the domain is simulated to reduce computational cost. The channel height to cylinder diameter ratio (H/D) is 1. The motion of a viscoelastic incompressible fluid is governed by a set of coupled equations including the conservation of mass, conservation of momentum, and a suitable constitutive model to describe the extra stress due to the viscoelasticity.

Continuity Equation

$$\nabla \cdot u = 0$$

Momentum Equation (Steady Navier-Stokes with Extra Stress)

$$\rho(u \cdot \nabla)u = -\nabla p + \eta_s \nabla^2 u + \nabla \cdot \tau$$

Where:

- ρ: fluid density
- p: pressure
- η_s : solvent (Newtonian) viscosity
- τ: polymeric (extra) stress tensor due to viscoelastic effects

Constitutive Equation – Oldroyd-B Model

$$\tau + \lambda \hat{\tau} = \eta_n (\nabla u + (\nabla u)^T)$$

Where:

- λ : relaxation time of the polymer
- η_p : polymer viscosity
- $\hat{\tau}$: upper-convected derivative of the stress tensor,

defined as:

$$\hat{\tau} = u \cdot \nabla \tau - (\nabla u)^T \cdot \tau - \tau \cdot \nabla u$$

Dimensionless Numbers

For the flow past a cylinder, two key dimensionless parameters are introduced:

• Reynolds number:

$$Re = \frac{\rho U_{avg}D}{\eta}$$

• Weissenberg number:

$$W_i = \lambda \frac{U_{avg}}{D}$$

- The viscosity ratio, defined as $\beta = \frac{\eta_s}{(\eta_s + \eta_p)}$, is fixed at 0.59.
- The drag coefficient is defined as

$$C_D = \frac{\int_{S} (\tau_{tot} - p\mathbf{I}) \cdot n \cdot \hat{\imath} \, dS}{\eta \cdot U_{avg}}$$

Boundary conditions:

At the inlet, a fully developed parabolic velocity profile is imposed, and a zero-pressure condition is specified at the outlet. No-slip boundary conditions are applied at the channel walls and along the cylinder surface.

Inlet (fully developed velocity and extra stress profile)

$$u(y) = (\frac{3}{2}U_{in}[1-(\frac{y}{H})^2], 0); \tau_{xx} = 2\eta_p W_i(\frac{\partial u}{\partial y})^2; \ \tau_{xy} = \eta_p \frac{\partial u}{\partial y}; \ \tau_{yy} = 0$$

Where:

- U_{ava} : average inlet velocity,
- H: half-channel height,
- η_p : polymeric viscosity,
- W_i : Weissenberg number.

Cylinder Surface and Channel Walls (no-slip condition)

$$u = 0$$

Centerline (Symmetry Boundary)

$$v = 0; \frac{\partial u}{\partial y} = 0; \frac{\partial \tau ij}{\partial y} = 0$$

Outlet (Zero normal stress condition)

$$\boldsymbol{\sigma} \cdot \boldsymbol{n} = -p_{out} \boldsymbol{n}$$

Assuming $p_{out} = 0$ this simplifies to:

$$\sigma \cdot n = 0$$

Where $\sigma = -pI + \eta_s(\nabla u + \nabla u^T) + \tau$ the total stress tensor and n is the outward normal.

The Finite Element Method is used to perform the numerical simulation of the steady-state viscoelastic flow past a circular cylinder was conducted using. The domain was discretized using a mapped mesh, with refined elements around the cylinder. Quadrilateral elements with quadratic interpolation for velocity and linear for pressure were used in the mixed finite element discretization (Owens & Phillips (2002)). An extra fine mesh (Figure 1b) was used near boundaries (especially the cylinder surface) to ensure numerical stability and convergence of the viscoelastic stress tensor. A mixed interpolation scheme that satisfies the incompressibility condition was employed. This higher-order velocity approximation provides enhanced accuracy in resolving the sharp elastic stress layers around the cylinder. The refined mesh near solid boundaries (an "extra fine" region at the cylinder wall) ensures that the polymeric stress tensor is well-resolved and minimizes numerical error in those critical highstress zones. The study was conducted, using a segregated solver and a parametric study is performed (Wi from 0 to 1) and (Re from 0.001 to 1). A fully coupled direct solver was used to solve the nonlinear system of equations. No special equation manipulation (e.g., a log-conformation formulation (Harlen et al. (1990)) was necessary, as the constitutive equations were solved in their original form given the moderate Wi range considered. Simulations were performed on multiple mesh densities to ensure convergence. In particular, halving the element size near the cylinder changed the computed drag coefficient by less than 1%, and the stress profiles showed negligible differences. This gives confidence that the chosen mesh (Fig. 2b) provides mesh-independent results for key quantities.

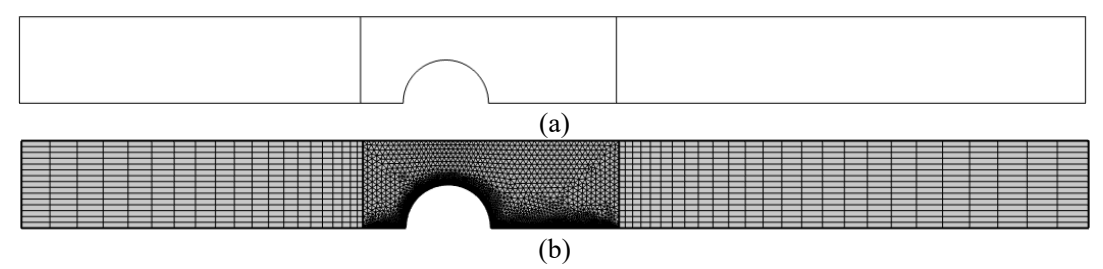


Figure 1. (a) considered geometry and (b) used Mesh.

3. MESH SENSITIVITY TEST AND CODE VERFICATION

Figure 2 present the effect of mesh elements number on Cd for Wi = 0 and 0.5. In both flows, Cd approaches an asymptotic value as the mesh is refined, with only minor changes beyond 5745 elements; this indicates that the solution becomes essentially grid-independent at sufficiently high mesh densities. Based on these results, a mesh comprising 5745 elements was selected to elaborate the numerical results while ensuring accuracy and avoiding the excessive computational cost. As shown in Table 1, the computed Cd at Re = 1 for Wi = 0.6–1.0 are in close agreement with the published data of Oscar et al. (2007). The present CFD results consistently yield slightly higher Cd values than the reference, with differences under 1%. The alignment between the present results and the benchmark data in Table 1 confirms the reliability and accuracy of the CFD model in predicting drag for viscoelastic flows.

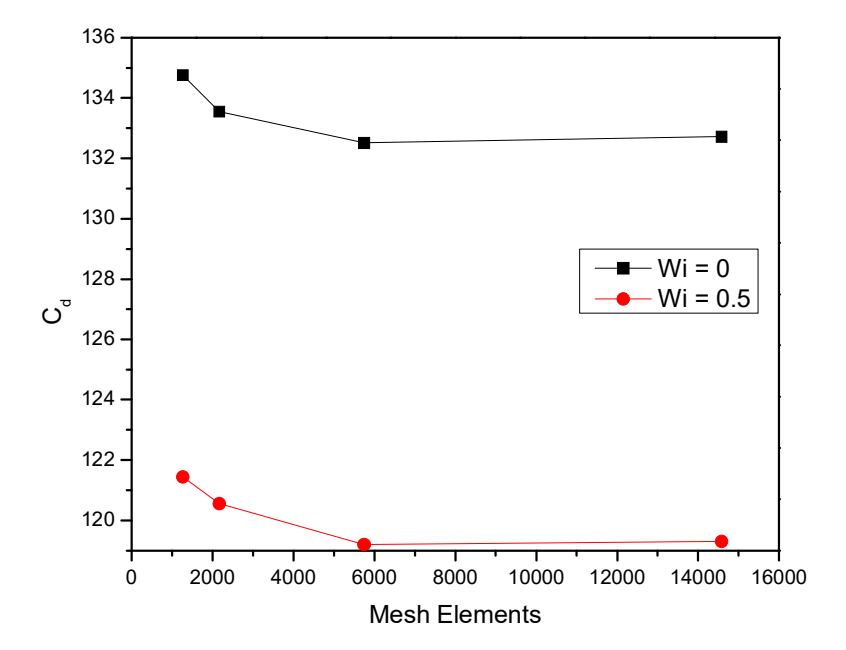


Figure 2. Mesh sensitivity test.

Table 1. Comparison of the results of Cd with those of Oscar et al. (2007), for Re = 1 and various Wi values.

Wi	0.6	0.7	0.8	0.9	1
Oscar et al. (2007)	117.84	117.39	117.41	117.78	118.43
Present results	118.26	117.91	118.05	118.66	119.58

4. RESULTS AND DISCUSSION

In this section, the results of the CFD study are presented, in term of velocity magnitude, extra stress lines. normal stress profiles and drag coefficient. In addition, a nonlinear regression model for the drag coefficient is performed, by establishing a correlation and evaluating the accuracy of the model using Residuals vs. Predicted plot, Actual vs. Predicted scatters, histogram of residuals and a normal QQ plot. For the presented results, the velocity magnitude is nondimensionalized by U_{avg} ; stresses are nondimensionalized by the characteristic viscous stress $\eta.U_{avg}/D$; and pressures are normalized by ρU_{avg}^2 . Figure 3 shows the computed flow field for three Reynolds numbers (Re = 0.01, 1, and 5) as the fluid elasticity (Wi) is varied from 0 (Newtonian) to 1. The color contours indicate velocity magnitude and the gray lines show the polymeric extra stress. At low Re = 0.01 the flow is nearly symmetric with essentially no wake, whereas at Re = 1 a clear recirculating wake forms; by Re = 5, the higher inertia produces an even longer, more pronounced wake behind the cylinder. As Wi increases, elastic stresses grow and noticeably alter the flow: the gray stress isolines become stronger and extend farther downstream, particularly at Re = 5 where the wake is longest. In particular, higher Wi produces large

normal stresses in the wake, corresponding to stretched polymer chains. Physically, this indicates that fluid elements are strongly pulled into extensional flow behind the cylinder. Concomitantly, the high-velocity (red) region narrows and the wake size is reduced with increasing Wi, even at Re = 5. These changes imply that elasticity suppresses large recirculating vortices (consistent with reported reduction of vortex size due to viscoelasticity) and tends to stabilize the wake, even in flows with moderate inertia (Re up to 5). Thus, Fig. 3 illustrates the interplay of inertia and elasticity: at low Wi the flow is dominated by inertia, resulting in a broad wake (more pronounced at higher Re), while at high Wi the buildup of elastic stresses confines the flow, yielding a thinner, more stress-dominated wake even at Re = 5.

Figure 4 presents pressure contours around the cylinder at Re=1 for increasing Wi. At Wi=0, the classic Newtonian pattern appears: a high stagnation pressure in front of the cylinder and a low-pressure wake behind. As elasticity grows, the pressure field changes: the upstream stagnation pressure increases and the low-pressure region contracts. This reflects the additional normal stress from stretched polymers, which effectively adds to the pressure on the cylinder surface. In Fig. 4 the contours become more uniform for higher W_i , indicating that the adverse pressure gradient behind the cylinder is weakened. In other words, viscoelastic normal stresses redistribute pressure around the cylinder. This tends to suppress flow separation, consistent with the confined wake seen in Fig. 3. The net effect is a flattening of the pressure distribution with Wi; the maximum pressure at the front rises and the downstream suction is reduced, which in turn influences the drag force on the cylinder. Such a shift in pressure pattern is a signature of elasticity. In fact, the normal stress variations directly modify the pressure field and thereby alter drag.

Figure 5 quantifies the buildup of elastic stress by plotting the longitudinal normal stress component (τ_{xx}) along the cylinder surface and along the wake centerline for Re = 0.01, 1, and 5. Each curve corresponds to a different Wi (0 to 1 by 0.1). In all cases, a sharp peak appears near ≈ 2 (stagnation at the front surface), and a secondary peak appears further downstream in the wake, with the wake peak occurring slightly farther downstream at higher Re. At Wi = 0 the stress levels are small, but as Wi increases the stagnation peak grows dramatically, reflecting intense extensional stress as fluid decelerates at the front. The wake peak likewise rises with Wi, growing more rapidly at Re = 1 than at Re = 0.01. For Re = 5 the increase is more tempered relative to the stagnation peak, this indicates that higher inertia moderates the relative growth of the downstream stress. Notably, at high Wi the wake peak surpasses the surface peak for Re = 1, indicating that the longest polymer stretches occur in the downstream wake; by contrast, at Re = 5 this disparity is less pronounced, with the stagnation and wake peaks becoming more comparable in magnitude. This behavior mirrors classic viscoelastic flows, where two distinct stress maxima arise: one in the boundary layer and one in the wake. The largest stresses occur at the front stagnation and along the centerline in all cases. The pronounced increase in τ_{xx} with Wi signifies that polymer elasticity leads to significant tensile stress buildup; at Re = 1 the wake stresses become much larger (and extend farther downstream) than at Re = 0.01, showing that even modest inertia amplifies the elastic wake. Conversely, raising Re to 5 yields no further increase in the peak stresses (the wake intensity remains similar to or slightly lower than at Re = 1), suggesting that beyond moderate inertia the elastic wake amplification saturates or even diminishes. In summary, Fig. 5 demonstrates that rising Wi causes extreme stress accumulation at the cylinder and in its wake for all the Re considered, underpinning the flow modifications seen in Figs. 3-4 and ultimately affecting the drag. Notably, the simulation captures key viscoelastic flow features – including a two-peak (bimodal) normal stress profile around the cylinder and the emergence of a downstream "negative wake" at high Wi (Chhabra & Richardson (1999)), across this range of Reynolds numbers.

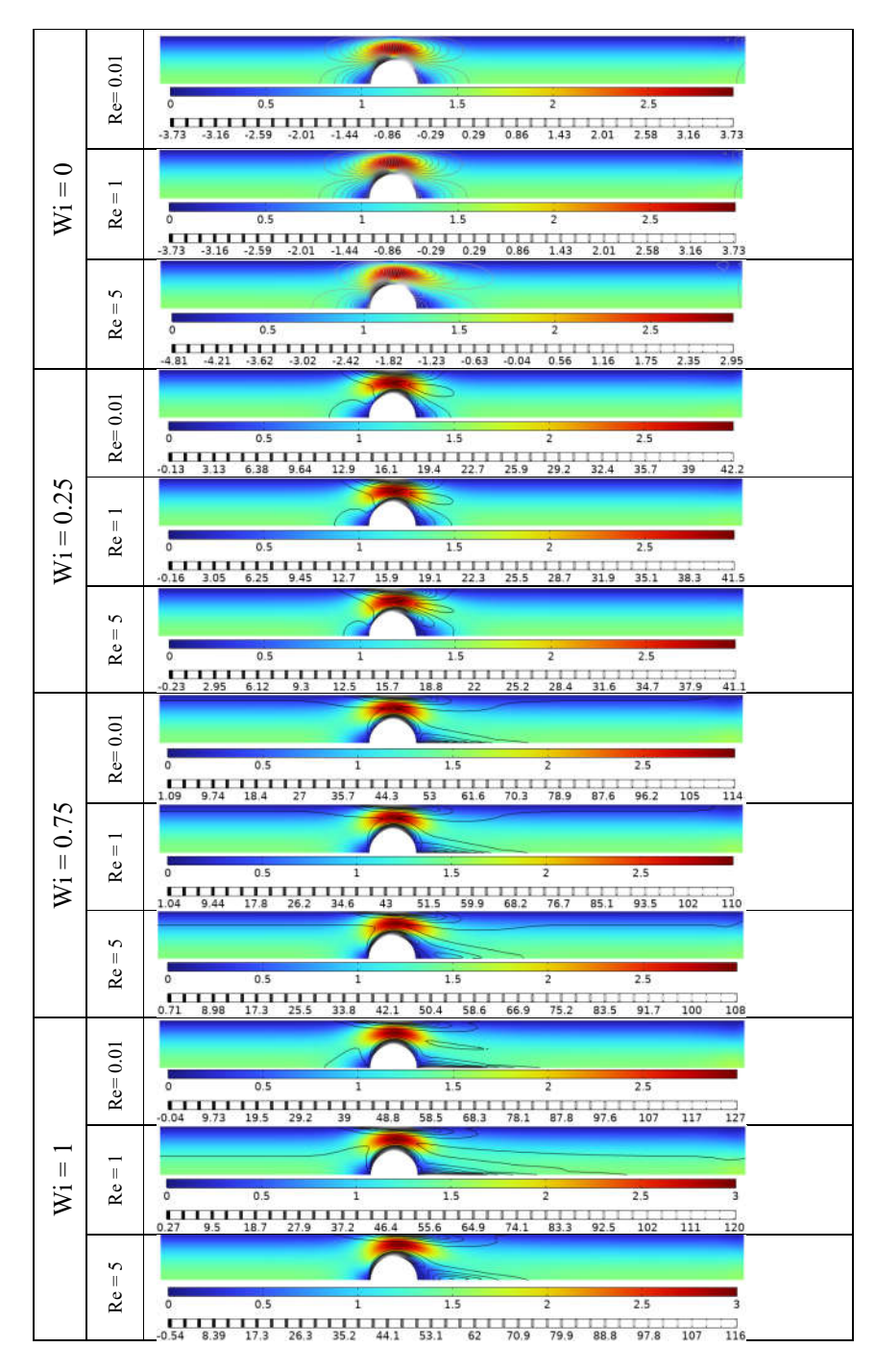


Figure 3. Effect of Wi and Re on the velocity magnitude (colored) and longitudinal normal stress τ_{xx} (gray) for $\beta = 0.59$.

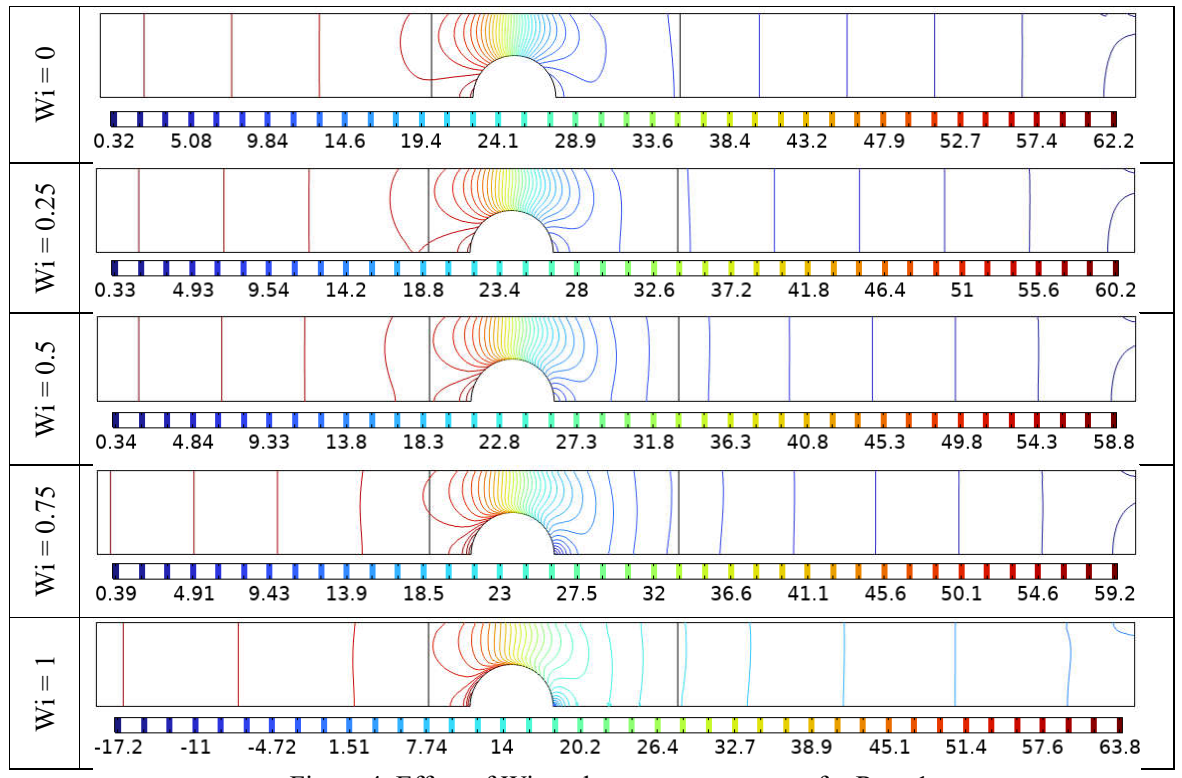


Figure 4. Effect of Wi on the pressure contours for Re = 1.

Figure 6 summarizes these effects in a quantitative drag coefficient (Cd) plot as a function of Wi, for Re = 0.01, 1 and 5. All curves show a very similar trend: Cd starts high at Wi = 0 and steadily decreases as Wi increases up to about 0.6, then rises slightly toward Wi = 1. Physically, this initial drop in drag indicates that moderate elasticity streamlines the flow and reduces resistance, with a minimum drag occurring around Wi ≈ 0.6 in each case. Beyond this point, further increases in Wi produce a slight drag rise, at very high elasticity the large polymer normal stresses push fluid toward the cylinder's rear, raising the pressure there and thus increasing drag. This characteristic behavior (an initial drag reduction followed by a modest rise) is in line with prior studies showing that viscoelasticity can first lower Cd at low-to-moderate Wi and then cause a slight rebound at high Wi. The inertia effect becomes more important for Re = 5. The Cd (Wi) curve for Re = 5 remains at higher values (i.e. greater drag) across the entire Wi range, and the elasticity-induced drag reduction is more subdued compared to the lower-Re cases. In other words, although at Re = 5 the Cd still drops to a minimum near Wi \approx 0.6, the dip is less pronounced, the minimum Cd is not as low (relative to the Newtonian value) as it is for Re = 0.01or 1, due to the counteracting effect of inertia. By contrast, the Re = 0.01 and Re = 1 curves nearly overlap, indicating that in this creeping-to-low Re regime the drag is governed primarily by elastic effects with negligible inertial influence. Figure 6 confirms that the increase of the elasticity, reduces the drag up to an intermediate Wi for all cases, but at higher Reynolds number (Re = 5) the balance between elastic and inertial forces moderates the extent of drag reduction while preserving the overall trend. The computed drag coefficients on the finest mesh closely match benchmark literature values (Owens & Phillips (2002) and Harlen et al. (1990)), confirming that the mesh resolution is adequate and validating the numerical results.

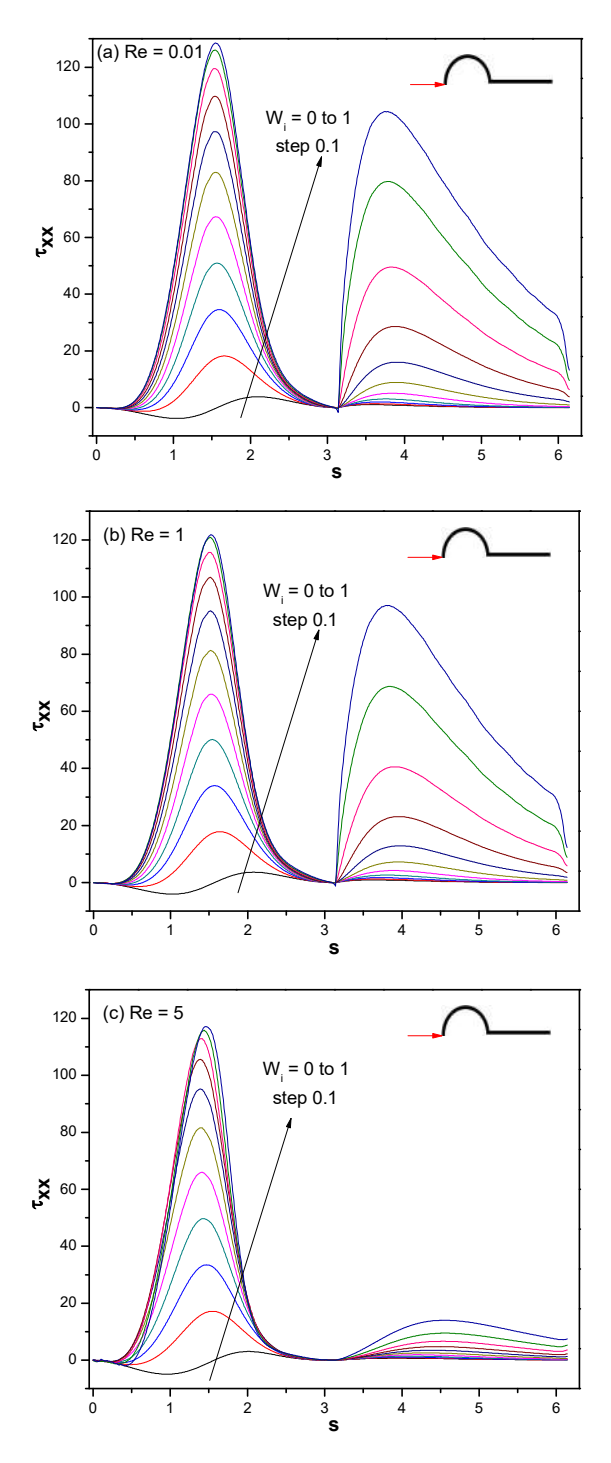


Figure 5. Profiles of longitudinal normal stress $(\tau_{\chi\chi})$ along the cylinder surface and wake centerline, for various Wi and Re values.

The computed drag coefficients for an Oldroyd-B fluid agree well with previously published data. Notably, the trend of drag reduction with increasing Wi, followed by a slight rebound at the highest Wi, matches the benchmark studies. Coronado et al. (2007) and others have reported that for a viscoelastic (Oldroyd-B) flow past a cylinder (with solvent viscosity ratio $\beta \approx 0.59$), the drag force monotonically decreases as Wi rises from 0 to about 0.6, reaching a minimum, and then levels off or increases slightly as Wi approaches the stability limit. In the current simulations, the same behavior is observed: for example, at Wi = 0.6 the drag coefficient is reduced by roughly 10–20% compared to the Newtonian case, and by Wi = 1.0 a slight increase in drag is seen. This non-monotonic drag pattern is in excellent agreement with prior numerical results.

Beyond the parameter range examined here, purely elastic instabilities are known to arise in viscoelastic wake flows. McKinley et al. (1993) observed that a steady wake becomes unstable once the ratio of elastic stresses to inertial and viscous forces approaches an order-unity threshold, and Pakdel & McKinley (1996) derived a corresponding dimensionless criterion indicating the onset of instability at Wi \approx 1 for flows with curved streamlines. Our simulations were restricted to Wi \leq 1, and no signs of unsteady or oscillatory behaviour were observed. Nevertheless, these criteria suggest that steady analysis would be invalidated once Wi significantly exceeds unity, as the flow would likely become unstable.

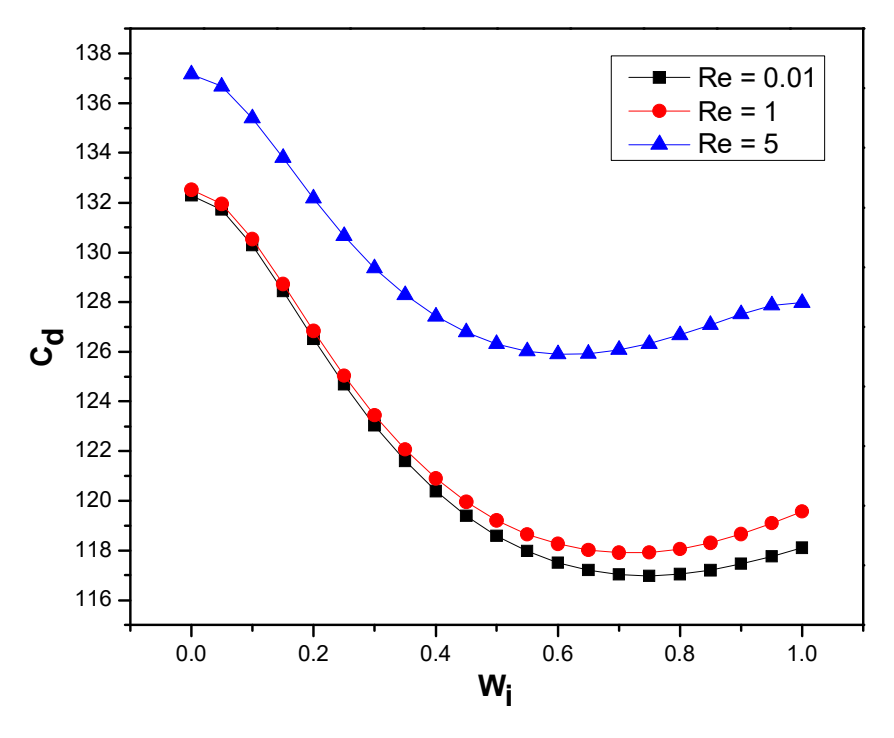


Figure 6. Effect of Wi on the Drag coefficient.

Regression analysis

A nonlinear regression analysis was conducted, to establish a rapid and accurate prediction of C_d, a regression model is developed based on the CFD simulation results. Among the tested models, an extended nonlinear expression of the form was selected due to its highest accuracy: $C_d = a \cdot Re^b + c \cdot W_i^d + f \cdot Re \cdot W_i^d + g \cdot Re^2 + h \cdot W_i^2 + e$

$$C_d = a \cdot Re^b + c \cdot W_i^d + f \cdot Re \cdot Wi + g \cdot Re^2 + h \cdot W_i^2 + e^2$$

with fitted parameters: a = 191.5557; $b = -5.8221 \times 10^{-5}$; c = -54.1039; d = 1.1629; f = 1.1777; g = -54.1039; d = 1.1629; d0.1898; h = 39.8277 and e = -58.5961 provided the best fit, with a coefficient of determination R^2 = 0.99586. in addition, accuracy of the model was validated through: MSE = 0.1184, RMSE = 0.34409, and MAE = 0.29211, These low values, with high R^2 , confirm that the validity of the predictive model. To capture the drag trends observed above, Figures 7-10 evaluate the accuracy of a fitted regression model predicting Cd from Wi and Re. Figure 7 plots the CFD-computed Cd (horizontal axis) against the model's predicted Cd (vertical axis) for all data points, with a reference 45° line indicating perfect agreement. The data points are very close to the ideal-fit line, indicating an excellent fit. Thus, it can be mentioned that the established regression model captures almost perfectly the complex non-linear dependence of drag on Wi and Re. In short, Fig. 7 provides visual confirmation that the regression model reproduces the CFD drag results with very high fidelity.

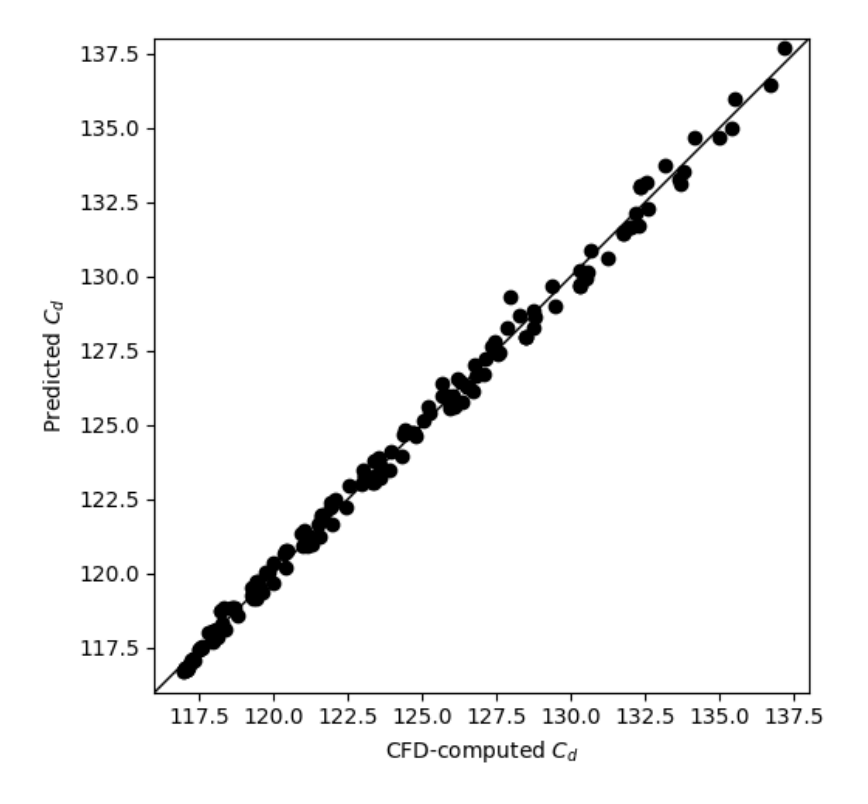


Figure 7. Actual Vs predicted C_d.

Figure 8 shows the residuals plotted against the predicted Cd. The points scatter randomly around the zero-residual horizontal line (red dashed). Importantly, there is no visible pattern or systematic trend in the scatter: no curvature, funnel shape, or clustering. Practically, a random scatter implies that the model errors are homoscedastic (constant variance) and uncorrelated with the predictions. This indicates that regression has captured all systematic effects and is not missing any structure.

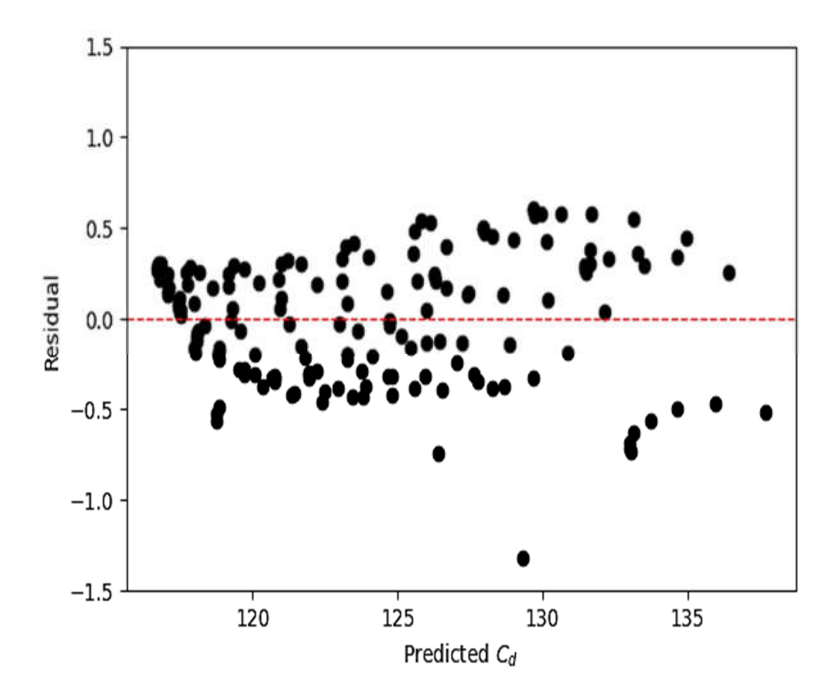


Figure 8. Residuals vs. Predicted Cd.

The histogram of residuals (Figure 9) allows the evaluation of the distribution of prediction errors. The histogram is symmetric, with bell-shaped pattern centered approximately at zero, suggesting that the residuals have a normal distribution. This behavior reinforces the statistical validity of the model. Most residuals are concentrated around the mean, indicating the rarity of large deviations, and the reliability of the model in capturing the drag behavior.

Finally, Fig. 10 is a quantile–quantile (Q–Q) plot of the residuals against a theoretical normal distribution. The residual points lie very close to the red reference line throughout the range of quantiles. This near-linearity demonstrates that the residuals follow a normal distribution very closely. In statistical diagnostics, such alignment confirms the normality of errors, an assumption underlying regression inference. Together with the histogram in Fig. 9, the Q–Q plot in Fig. 10 shows that the model's error distribution satisfies the normality assumption. In summary, Figs. 7–10 collectively validate that the regression model accurately predicts Cd: the high R2 and the well-behaved residuals indicate the model is both precise and unbiased across the studied Reynolds and Weissenberg number range.

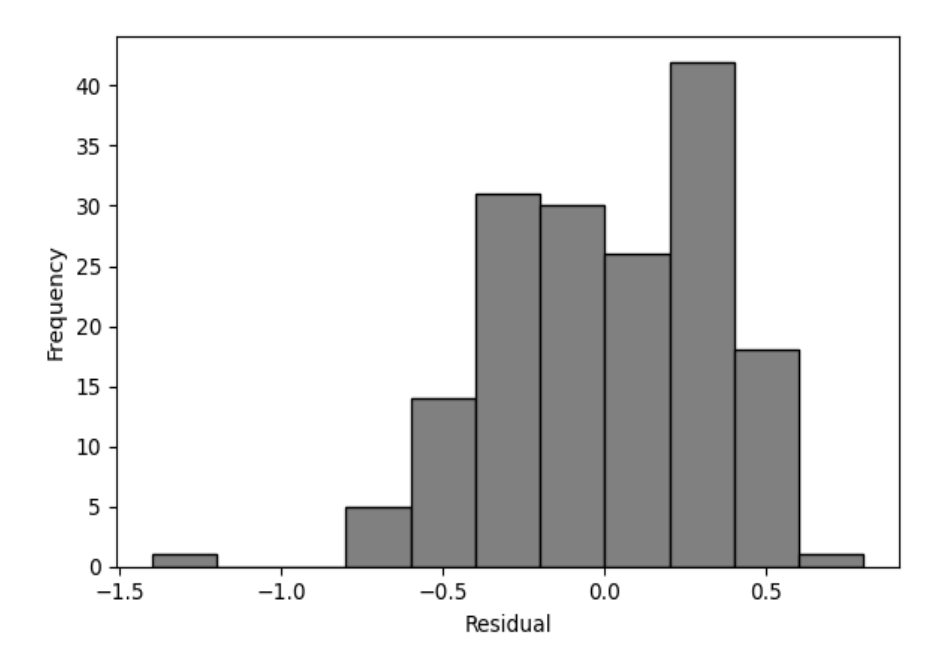


Figure 9. Histogram of residuals.

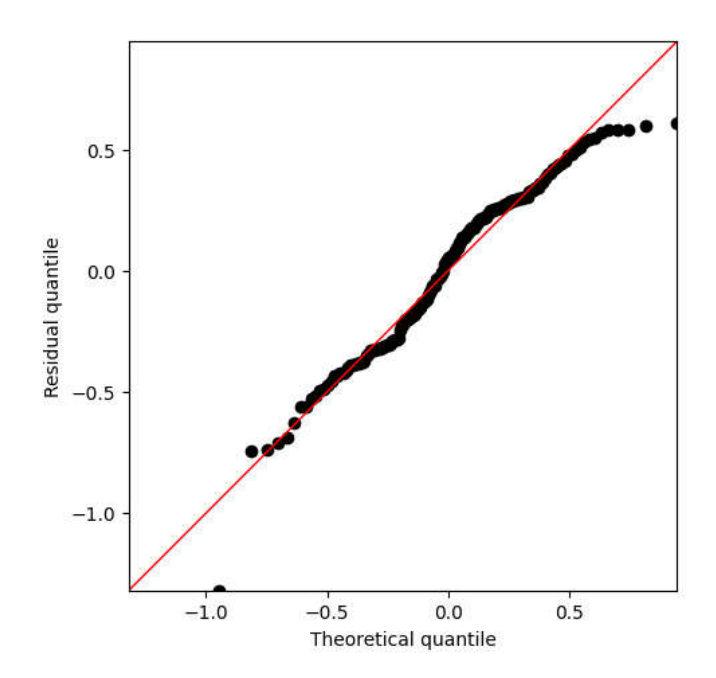


Figure. 10: Q-Q Plot of Residuals.

5. CONCLUSION

The CFD results provide clear physical insight into viscoelastic flow past a cylinder at low Reynolds numbers. Increasing polymer elasticity drives up the rear-stagnation pressure and shifts the wake, yielding a notable reduction in form drag up to moderate Wi. In our simulations the drag coefficient dropped significantly (by roughly 10–20%) as W_i increased to about 0.6; beyond this point further elasticity caused a minor drag increase, due to extremely large elastic stresses. The extra polymeric stress is highly concentrated on the cylinder surface and along the wake centerline, producing two peak τ_{rr} values. These stress patterns and the altered pressure field explain the observed drag reduction trend. Building on the CFD database, we transitioned to a data-driven modeling step by fitting a nonlinear multivariable regression to the drag results. The chosen regression form accurately captures the dependence of C_d on Re and W_i , with fitted parameters yielding $R^2 = 0.99586$, MSE = 0.1184, RMSE = 0.34409, MAE = 0.29211 over the entire dataset. The residual analysis showed no systematic bias or nonlinearity, confirming the statistical validity of the model. In summary, this work demonstrates that a high-fidelity Oldroyd-B CFD study combined with a tailored regression can both uncover fundamental flow physics and deliver a fast surrogate model. The compact regression model enables rapid drag estimation across the studied Reynolds-Weissenberg range, making it useful for reduced-order analyses or parametric design studies where full CFD would be too costly. Thus, the CFD-data synergy provides both insight and practical value for predicting viscoelastic cylinder drag.

References

Baaijens, F. P., et al. (1997). Viscoelastic flow around a restricted cylinder of low-density polyethylene melt. Journal of Non-Newtonian Fluid Mechanics, 73(1-2), 181-187.

Binding, D. M., & Walters, K. (1988). Utilizing flow through a contraction to estimate the extensional viscosity of mobile polymer solutions. Journal of Non-Newtonian Fluid Mechanics, 30(2-3), 233-250.

Bird, R. B., et al. (1987). Dynamics of Polymeric Liquids, Volume 2: Kinetic Theory. Wiley-Interscience.

Bonn, D., et al. (2004). Yield stress materials in soft condensed matter. Reviews of Modern Physics, 76(1), 1-24.

Chhabra, R. P., & Richardson, J. F. (1999). Non-Newtonian Flow and Applied Rheology. Butterworth-Heinemann. Coronado, O. M., Arora, D., Behr, M., & Pasquali, M., Asimple method for simulating general viscoelastic fluid flows with an alternate log-conformation formulation, J. Non-Newtonian Fluid Mech., 147 (2007) 189–199

Harlen, O. G., Rallison, J. M., & Chilcott, M. D. (1990). High Deborah number flows of dilute polymer solutions. J. Non-Newtonian Fluid Mech., 34(3), 319–349.

Harlen, O. G., et al. (1990). High Deborah number flows of dilute polymer solutions. Journal of Non-Newtonian Fluid Mechanics, 34(3), 319-349.

Keunings, R. (1986). On the high Weissenberg number problem. Journal of Non-Newtonian Fluid Mechanics, 20(2), 209-226.

Larson, R. G. (1992). Instabilities in viscoelastic flows. Rheologica Acta, 31(3), 213-263.

McKinley, G. H., & Hassager, O. (1999). The Consideré condition and rapid stretching of dilute polymer solutions. Journal of Rheology, 43(5), 1195-1212.

McKinley, G.H., Armstrong, R.C., & Brown, R.A. (1993). The wake instability in viscoelastic flow past confined circular cylinders. Philosophical Transactions of the Royal Society of London. Series A: Physical and Engineering Sciences, 344(1671), 265–304.

Oscar M. Coronado, Dhruv Arora, Marek Behr, Matteo Pasquali, A simple method for simulating general viscoelastic fluid flows with an alternate log-conformation formulation, J. Non-Newtonian Fluid Mech. 147 (2007) 189–199.

Owens, R. G., & Phillips, T. N. (2002). Computational Rheology. World Scientific.

- Pakdel, P., & McKinley, G.H. (1996). Rheological and geometric scaling of purely elastic instabilities. Journal of Non-Newtonian Fluid Mechanics, 67, 19–47.
- Pearson, J. (1985). Instabilities in flow of viscoelastic fluids. Annual Review of Fluid Mechanics, 17(1), 159-185. Phan-Thien, N., & Tanner, R. I. (1977). A new constitutive equation derived from network theory. Journal of Non-Newtonian Fluid Mechanics, 2(4), 353-365.
- Poole, R. J., & Escudier, M. P. (2009). Turbulent flow of viscoelastic fluids. Journal of Non-Newtonian Fluid Mechanics, 157(1-2), 1-9.
- Rallison, J. M., & Hinch, E. J. (1988). Do we understand the physics in the constitutive equation? Journal of Non-Newtonian Fluid Mechanics, 29(1-3), 37-55.
- Shaqfeh, E. S. G. (1996). Purely elastic instabilities in viscometric flows. Annual Review of Fluid Mechanics, 28(1), 129-185.
- Sun, Z., et al. (2014). Drag reduction of viscoelastic fluids around bluff bodies. Physics of Fluids, 26(3), 035105. Tanna, H. K., & Zaki, T. A. (2016). Pressure fluctuations in viscoelastic channel flows. Journal of Fluid Mechanics, 788, 327-351
- Tropea, C., et al. (2007). Springer Handbook of Experimental Fluid Mechanics. Springer.
- White, C. M., & Mungal, M. G. (2008). Mechanics and prediction of turbulent drag reduction with polymer additives. Annual Review of Fluid Mechanics, 40, 235-256.
- Zhang, M., et al. (2014). Numerical simulations of viscoelastic flow using regression models. Computers & Fluids, 103, 167-176.